



Effect of a Trifluorophenyl-Based Monomer on the Electro-optic Performances of Polymer-Stabilized Blue Phase Liquid Crystals

Minggang Hu¹ · Jiangwei Li¹ · Nejmaddin Avci²

Received: 24 June 2020 / Published online: 15 September 2020
© Sociedade Brasileira de Física 2020

Abstract

We synthesized one novel mono-functional acrylate monomer. The effect of the new monomer on blue phase liquid crystal stabilization and electro-optical properties was investigated with different reactive polymer concentration and combination. The temperature range of blue phase samples was widened over 50 °C including room temperature through the use of polymer stabilization. Electro-optical properties including lower driving voltage (69.8 V), lower hysteresis (3.9%), lower response time (0.468 ms), and higher Kerr constant (9.4 nm/V²) were obtained by optimizing the concentration of different composites. They are strongly influenced by the interface energy between the liquid crystal molecules and polymer combination system. It is found that hysteresis is sensitive to the polymer concentration.

Keywords Polymer blue phase · Liquid crystal · Monomer · Response time · Hysteresis · Kerr constant

1 Introduction

Blue phases (BPs) are usually found only in a narrow temperature range of a few degrees between the isotropic liquid and the helical cholesteric phases with a relatively short helical pitch [1, 2]. In general, they can be divided into three distinct thermodynamic phases depending on the double-twisted cylinder packing structure (neighboring molecules slightly twist into each other to constitute a helicoidal twist) as functions of temperature and chirality: blue phase I (BP I), blue phase II (BP II), and blue phase III (BP III). The packing structure of BPI and BPII is body-centered cubic lattice and simple cubic lattice, respectively. In contrast, BPIII possesses almost the same symmetry as the isotropic phase.

BPs are potentially considered as candidate materials for next-generation electro-optic and photonic application owing to the electrically controllable Bragg diffraction of visible light such as fast optical shutters and photonic applications [3, 4]. Since they show fast electro-optic effect characterized by optical switching between isotropic and anisotropic states,

nevertheless, their narrow temperature range is an important problem. To date, tremendous research efforts have been successfully made to broaden the temperature range of BPs as well as to shift them towards the room temperature. The first successful experimental approach was reported by Kikuchi et al. [4]. A small amount of specific reactive monomer (~ 10 wt%) tends to selectively concentrate in the lattice disclination lines of the BP and hence stabilize the overall cubic lattice against the temperature variation and electrical field. Therefore, the temperature range of the polymer-stabilized BPI is extended to more than 50 K, including room temperature with an ultrafast response time. It is termed as polymer-stabilized blue phases (PSBPs). Its electro-optical response time is of the order of 0.1 ms. The mechanism of BP stabilization contains the localization of polymer chains into the disclinations that lower the effective free energy. Another alternative methods of extending the temperature range of BPs are the use of eutectic mixtures of three homologs of a symmetrical dimmer molecules possessing a large flexo-electric coefficient [5], spherical or anisotropic nanoparticles [6–10], a combination of polymer and nanoparticles [6], hydrogen-bonded self-assembled LC complexes [11, 12], T-shaped chiral oligomer molecules [13], bent-shaped molecules [14–18], binaphthyl derivatives [19], light induction [20], discotic molecules [21], inorganic perovskite quantum dots [22], and reduced graphene oxide [23, 24] as stabilization agents.

✉ Nejmaddin Avci
navci@mu.edu.tr

¹ Xi'an Modern Chemistry Research Institute, Xi'an, China

² Faculty of Science, Department of Physics, Mugla Sitki Kocman University, 48000 Kotekli, Mugla, Turkey

Polymer-stabilized blue phase liquid crystal (PSBPLC) has unique physical properties; optical isotropic status in the absence of electric field, sub-millisecond response (which is $\sim 10 \times$ faster than a typical nematic), large optical Kerr effect, optically active, wide viewing angle without any compensation films, lack of requirement of any surface alignment layer, and cell gap insensitivity, both of which facilitate fabrication processes and lower cost. However, high switching voltage, voltage-induced hysteresis, light scattering and residual transmittance, and long-term stability are still big challenge on the road toward practical applications [25–28]. Three methods could be considered for lowering voltages: (1) thrive a LC material with a large Kerr constant; (2) design electrode shape, structure, and dimension for creating strong and deep-penetrating electric fields; and (3) optimize the monomer/LC compositions (monomer types, monomer concentration, and monomer ratio).

So far, numerous efforts to improve these problems have been carried out in terms of device and materials based on BPLC [25–61]. Alternative way to reduce high operating voltage is the synthesis of new polymeric materials such as reactive monomers with different functionalities. To the best of our knowledge, the effects of fluoro-content monomers (with a stronger dipole moment) which may possess substantial effect on the properties of the PSBPLCs have seldom been investigated [42, 43]. According to the literature, the partial replacement of fluoroacrylates in the monofunctional monomer composition induced a decrease in the free energy of PSBPLC on account of low surface tension of fluorinated polymer [42].

In present paper, we synthesized a novel fluorinated monomer, 3,4,5-trifluorophenyl 4-((6-acryloyloxy)hexyl)oxy benzoate, which can reduce the operating voltage of BPLCs. The electro-optical properties of BPLC stabilized with seven sets of monomer combination were investigated, which are involved in the stability, operating voltage, Kerr constant, hysteresis, and response time. The total concentration of monomers was controlled at around 10 wt% in order to clarify the effect of the newly synthesized reactive monomer, as well as the ratio between other monomers. In addition, the optimum monomer concentration with the synthesized monomer was investigated.

2 Characterization

The structures of the final products and intermediates were confirmed by a variety of spectral methods. Infrared spectrometry (IR) spectra were recorded on a Nicolet Avatar 360E spectrometer. ^1H -nuclear magnetic resonance (^1H NMR) with tetramethylsilane (TMS) as internal standard was recorded on a Bruker AV500 (500 MHz) instrument (Bruker Biospin Group, Fällanden, Switzerland). The mass spectra (MS) were

obtained by GC/MS Thermo DSQ (Thermo Fisher Scientific Inc., Waltham, MA, USA) with m/z 50–650.

3 Synthesis

The synthetic method of trifluorophenyl-based mono-functional acrylate monomer (AHFF) is illustrated as Scheme 1.

3.1 Materials

Ethyl 4-hydroxybenzoate, 3,4,5-trifluorophenol, and 6-chlorohexyl acetate were purchased from Wuxi Yangshi Chemical Co. Ltd. and used as received. 4-Dimethylaminopyridine (DMAP) and dicyclohexylcarbodiimide (DCC) were purchased from Zhejiang Bulk Chemical Co. Ltd.

3.2 Synthesis of Methyl Ethyl 4-[(6-Acetoxyhexyl)Oxy] Benzoate (f2)

Ethyl 4-hydroxybenzoate (7.3 g, 44 mmol) and 6-chlorohexyl acetate (9.97 g, 56 mmol) were dissolved in 200 mL of DMF; then, 13.8 g (100 mmol) K_2CO_3 and 8.3 g (50 mmol) KI were added to the solution. The mixture was refluxed for 4 h and then cooled to room temperature. After that, the mixture was filtered to remove the insoluble salts; a yellow solution was achieved. The solution was then dumped into 1000 mL of water under vigorous stirring for 1 h to obtain the white particles. Yield (12.8 g, 94%).

3.3 Synthesis of 4-[(6-Hydroxyhexyl)Oxy]Benzoic Acid (f3)

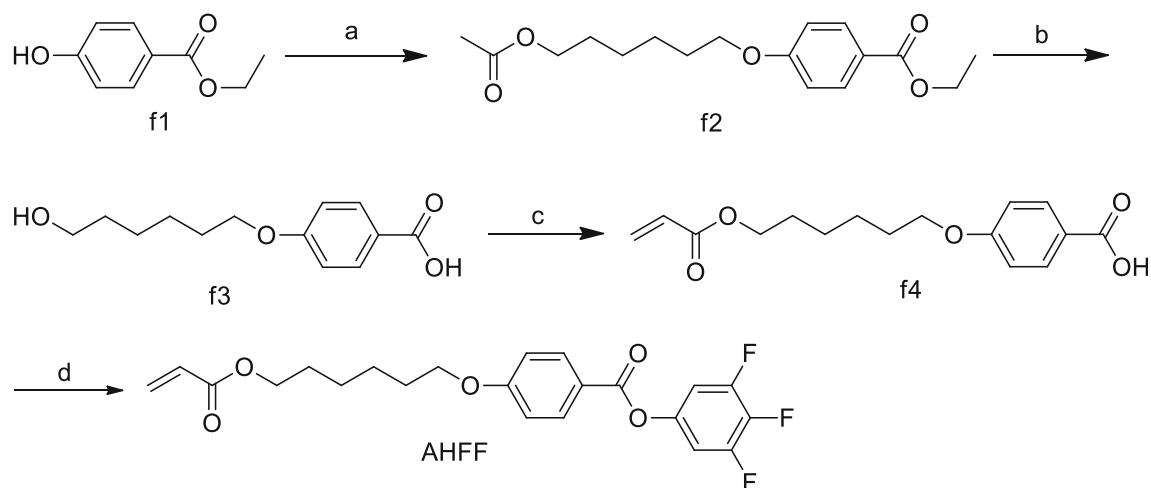
Ethyl 4-[(6-acetoxyhexyl)oxy]benzoate (12.8 g, 41.5 mmol) was added to a three-necked bottle followed by 50 mL water, 50 mL EtOH, and 5.6 g (140 mmol) NaOH. The mixture was refluxed for 8 h, and then cooled to room temperature. Concentrated HCl (20 mL) was added to the solution; the white precipitation was filtered and purified by recrystallization with EtOH. Yield (9.12 g, 87%).

IR (ν/cm^{-1}): 3338, 2952, 2859, 2530, 1866, 1670, 1597, 1577, 1505, 1417, 1284, 1258, 1170, 1005, 1119, 1057, 965, 846, 774, 728, 645, 506.

^1H -NMR (500 MHz, DMSO) δ = 12.58 (s, 1H), 7.90–7.85 (m, 2H), 7.03–6.97 (m, 2H), 4.34 (t, J = 5.1 Hz, 1H), 4.06–3.99 (m, 2H), 3.39 (m, 2H), 1.81–1.66 (m, 2H), 1.50–1.28 (m, 6H).

3.4 Synthesis of 4-[(6-(Acryloyloxy)Hexyl)Oxy]Benzoic Acid (f4)

4-[(6-hydroxyhexyl)oxy]benzoic acid (9.12 g, 38.3 mmol) and 7.24 g (60 mmol) *N,N*-dimethylaniline were added to



Scheme 1 Synthetic method for preparation AHFF. **a** Ethyl 4-hydroxybenzoate, K_2CO_3 , KI, DMF, 94%. **b** NaOH, EtOH/H₂O, 87%. **c** N,N-dimethylaniline, acryloyl chloride, DCM, 94%. **d** DCC/DMAP, 3,4,5-trifluorophenol, DCM, 85%

100 mL DCM; the mixture was stirred for 1 h, and then, acryloyl chloride (4.16 g, 46 mmol) was dropped and stirred for 20 h. After that, 2 mL of concentrated HCl was added to the solution and stirred for 0.5 h, and then, the mixture was extracted and washed by 300 mL of water for three times. The organic phase was dried with $MgSO_4$ and evaporated to obtain the white solid. Yield (10.51 g, 94%).

IR (ν/cm^{-1}): 2940, 2862, 2669, 2555, 1732, 1696, 1696, 1691, 1607, 1514, 1466, 1430, 1295, 1248, 1196, 1175, 977, 764, 644, 555.

1H -NMR (500 MHz, DMSO): δ = 12.58(s, 1H), 7.87(m, 2H), 7.00(d, J = 8.8 Hz, 2H), 6.32 (m, 1H), 6.17 (m, 1H), 5.93 (m, 1H), 4.19–3.99 (m, 4H), 1.83–1.57 (m, 4H), 1.51–1.27 (m, 4H).

3.5 Synthesis of 3,4,5-Trifluorophenyl 4-[(6-(Acryloyloxy)Hexyl)Oxy]Benzoate (AHFF)

4-[(6-(acryloyloxy)hexyl)oxy]benzoic acid (2.92 g, 10 mmol), 4-dimethylaminopyridine (0.06 g, 0.5 mmol), and DCC (2.48 g, 12 mmol) were added in sequence to 20 mL DCM, and then, a solution of 30 mL DCM and 3,4,5-trifluorophenol (1.78 g, 12 mmol) was dropped and stirred for 20 h. The solution was filtered to remove the insoluble salts, then washed by HCl (5%) and aqueous Na_2CO_3 (5%) three times, respectively. The organic phase was dried with $MgSO_4$ and concentrated. The residue was purified by silica-gel column chromatography, and white solid was obtained. Yield (3.59 g, 85%).

IR (ν/cm^{-1}): 3071, 2952, 2864, 1726, 1644, 1639, 1608, 1597, 1525, 1453, 1413, 1273, 1237, 1206, 1170, 1134, 1057, 1041, 1011, 887, 851, 506.

1H -NMR (500 MHz, $CDCl_3$): δ = 8.12–8.06 (m, 2H), 6.99–6.86 (m, 4H), 6.40 (dd, J = 17.3, 1.3 Hz, 1H), 6.13 (dd,

J = 17.3, 10.4 Hz, 1H), 5.82 (dd, J = 10.4, 1.3 Hz, 1H), 4.18 (t, J = 6.7 Hz, 2H), 4.05 (t, J = 6.4 Hz, 2H), 1.89–1.80 (m, 2H), 1.76–1.68 (m, 2H), 1.58–1.42 (m, 4H).

^{13}C -NMR (125 MHz, $CDCl_3$): δ = 166.3, 164.1, 163.9, 152.1 (d, $^1J_{C-F}$ = 251 Hz, 2 C), 150.2, 137.0 (m, 1 C), 132.5, 130.6 (2 C), 128.6, 120.5, 114.5 (2 C), 107.3 (d, $^2J_{C-F}$ = 16 Hz, 2 C), 68.2, 64.4, 28.9, 28.5, 25.7, 25.6.

4 Experimental

4.1 Sample Preparation

The nematic LC host used in this study was commercially available eutectic nematic mixture HTG-135200 (HCCH, China). Its physical properties are $\Delta n = 0.205$ at $\lambda = 633$ nm, $\Delta \epsilon = 99$ at 1 kHz and 23 °C, a rotational viscosity, $\gamma = 1.2$ Pa · s (at 22 °C), the clearing temperature is 98 °C. The chemical structure of HTG-135200 is not available due to commercial confidentiality. In order to induce chirality into the host nematic LC, R5011 (HCCH) was used as a chiral dopant. The helical twisting power (HTP 120/ μm at 23 °C) of R5011 is dependent on the temperature. The chiral pitches were maintained at about 339 nm by adjusting the chiral concentration, since the electro-optical performance for PSBPLCs is dependent on their chiral pitch.

For the polymer stabilization of BP, monofunctional monomers used to form polymer networks in BPLCs were dodecyl acrylate (C12A, Wako) and 3,4,5-trifluorophenyl 4-((6-acryloyloxy)hexyl)oxy)benzoate denoted as AHFF. Bifunctional monomer was 2-methyl-1,4-phenylene bis(4-(3-(acryloyloxy)propoxy) benzoate (RM257, Merck) and trifunctional monomer was 1,1,1-

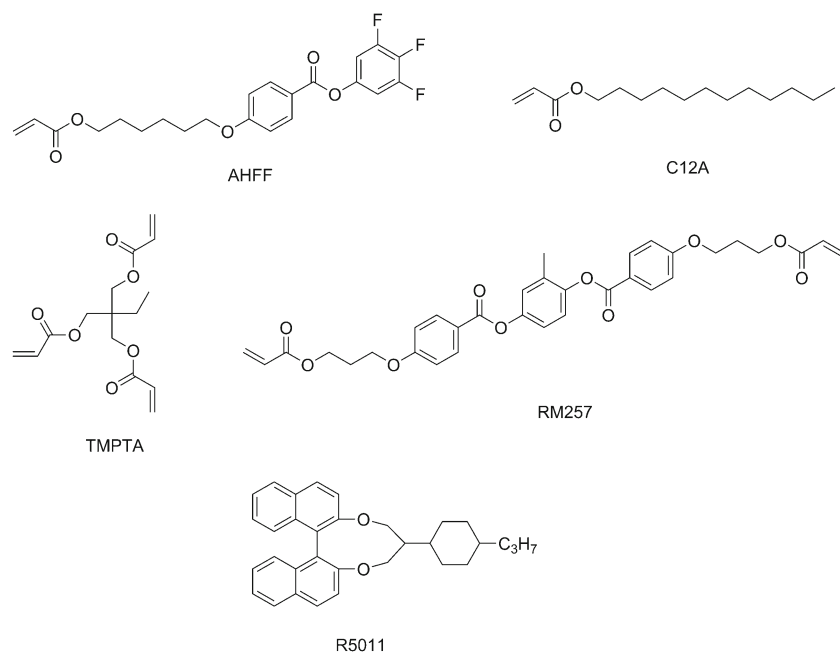


Fig. 1 Chemical structure of substituents

trimethylolpropane triacrylate (TMPTA, Sigma Aldrich). Difunctional acrylate has only nematic phase; neither the monofunctional acrylate nor trifunctional show mesophase. The chemical structure of the materials is given in Fig. 1. RM257 and AHFF are the main components for building the primary polymer skeletons in PSBPLC samples. The temperature range of a PSBPLC system is very much dependent on the mixing ratio, because each mixture possesses characteristically different behaviors such as Kerr constant, viscosity, and isotropic temperature.

To investigate the effects of monomer/LC compositions, seven precursors containing a variety of functional groups were prepared as shown in Table 1. All chemical stuff was used without any further treatment. On the other hand, the monomer concentration plays an important role in the stabilization of BPLC. Hence, the mixing ratios of monomers were altered to carry out the effect of monomer concentration on

BPLC stabilization. For comparison, the total polymer concentration was fixed at 10% by weight to prevent from affecting the properties of PSBPLC. Moreover, the concentration of RM257 was maintained at around 6% by weight in the precursors. The BPLC/monomer mixtures were mechanically blended at higher than the clearing point of the LC to form a homogeneous mixture for several times.

Each precursor was heated up to an isotropic state to prevent flow alignment, and then, it was filled into an empty in-plane-switching (IPS) cell without polyimide alignment layer by means of capillary force, since BPLCs are self-organized structures. The top substrate of the IPS cells has no electrode, but the bottom substrate has comb-type interdigitated indium tin oxide (ITO) electrodes. The electrode gap was 12 μm . The distance between the electrodes was 8 μm wide. The cell thicknesses of IPS cells were maintained between 7.24 and 7.35 μm by spacers. The cell thickness was measured by a UV-Vis-NIR spectrometer (HR2000, Ocean Optics). The

Table 1 The constituent fractions of the materials in order to prepare PSBPLCs

Precursors	HTG-135200 (wt%)	R5011 (wt%)	AHFF (wt%)	TMPTA (wt%)	C12A (wt%)	RM257 (wt%)
A1	85.76	4.25	3.98	0	0	6.01
A2	85.61	4.24	2.46	1.67	0	6.02
A3	85.76	4.27	2.96	1.07	0	6.04
A4	85.72	4.28	2.01	1.99	0	6.00
CB1	85.74	4.27	2.00	0	2.01	5.98
CB2	85.75	4.23	2.99	0	1.06	5.97
CB3	85.67	4.21	1.16	0	2.95	6.01

temperature was carefully controlled by a Linkam hot stage LTS350 and a controller TMS94 with an accuracy of $0.1\text{ }^{\circ}\text{C}$ to identify the temperature range of samples. Prior to polymer stabilization, the cells were stayed at thermal balance for 20 min, and then, they were cooled down from an isotropic state to the state of blue phase at a cooling rate of $0.1\text{ }^{\circ}\text{C}/\text{min}$ as slowly as possible to prevent super cooling, which is frequently viewed for a phase transition from a BP to the cholesteric phase. The phase transition temperatures and the optical texture of each sample were achieved by using a reflective polarizing optical microscopy (POM) equipped with a commercial hotplate (Linkam TMS 94). The samples exhibited BPs both heating and cooling processes in the absence of polymer-stabilization. The temperature of the precursors was adjusted very precisely to the appearance of the BP texture. After confirming that the whole sample showed the desired phase, the cells were illuminated (from the bare glass substrate side at normal incidence) with ultraviolet light (L2859–01, Hamamatsu Photonics LC6) with $8\text{ mW}/\text{cm}^2$ for 45 min at the BPI temperature range to form PSBPLC. Herein, the polymerizable monomer components move to the defect regions of LC (the disclinations) and nucleate at polymer chains in disclination lines to form the 3D BP periodic structure. After photo-polymerization, the samples were allowed to cool down to room temperature with the rate of temperature change $1\text{ }^{\circ}\text{C}$ per minute. Figure 2 shows the platelet textures of the chosen samples observed under the POM in the reflective mode at room temperature. BP samples exhibited characteristic selective light reflections in the visible wavelength range owing to Bragg diffraction from the cubic lattice. Their phase transition temperatures are listed in Table 2. A variety of mixing ratios of monomers were a significant influence on the thermal stability of BPs. In this way, they achieved a wide temperature range of more than 50 K that includes room temperature due to the formation of polymer chains localized into the disclination lines and pushing the low molecular weight LC out those lines [2–5]. This lowers the free energy related to these disclinations with high elastic energy and enhances the thermal stability of BP. Besides, the photo-polymerization increases the upper temperature for all samples.

4.2 Electro-optical Properties

Figure 3 depicts the experimental setup. To characterize the electro-optical properties, a linearly polarized He-Ne laser (about 1 mW at $\lambda = 633\text{ nm}$) was utilized as a light source. A lens is inserted between the PSBP cell and the photodiode detector to collect most of the diffraction orders into the photodiode. Transmittance with 100% was adjusted by that of the cell under parallel polarizers. Transmittance with 0% was set by that of the cell under crossed polarizers. To maximize the transmittance, azimuthal angle of the striped electrode was placed at an inclination angle of 45° with respect to incident

light. The transmitted light intensity was measured by a photodetector (New Focus Model 2031) connected to an oscilloscope (Tektronix TDS-2014). The cells were driven by a square-wave electric field with a frequency of 1 kHz put through an amplifier (FLC electronics, model F20) and was recorded digitally by a LabView data acquisition system. The voltage ramping rate was 500 ms per step. In the IPS cell, the electric field-induced birefringence was in the lateral direction to the plane of the substrate.

5 Results and Discussion

5.1 Driving Voltage

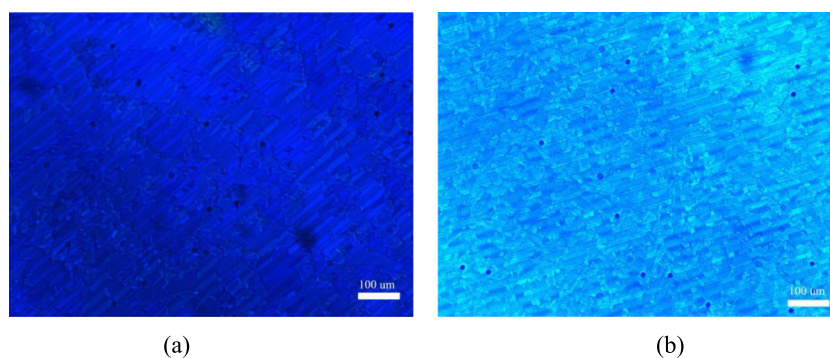
To evaluate the electro-optical properties, we measured voltage-dependent transmittance at different temperatures. Figure 4 demonstrates the normalized voltage-dependent transmittance curves (VT) from 23 to $60\text{ }^{\circ}\text{C}$ for A1. Transmittance without an electric field was 0%; BP is optically isotropic. This data may be approximately described by the relative transmitted intensity through a uniaxial birefringent slab

$$T_{\text{nor}} = \sin^2(2\Psi)\sin^2\left(\frac{\pi\Delta n_{\text{induced}}(E)d}{\lambda}\right) \quad (1)$$

Here, $\Delta n_{\text{induced}}$ is the induced birefringence at a particular applied voltage and Ψ is the angle of the induced, in-plane, optic axis with respect to either the polarizer or analyzer crossed axis. Ψ is equal to 45° in this study. The transmittance increased concomitantly with increasing of the electric field. The threshold-like voltage of the BPLC cell is around 10 V and the saturation voltage was 69.8 V for room temperature. Namely, the BP molecules aligned by electric field are increased with an increase of the applied electric field. Operating voltage (V_{ON}) is defined as a voltage at the maximum transmittance of the VT curve. As the temperature increases, V_{on} increases. This process was repeated for other samples. In an IPS cell, the electric field distribution across the electrode gap and cell thickness is not uniform spatially. The electrode dimension acts on a crucial role affecting the maximum optical transmittance and operating voltage. If the electrode spacing was reduced, the operating voltage would decrease in the IPS cells due to a stronger electric field and the decrease would be leveled by the increased electric field intensity and the thinner effective layer in the horizontal plane [29–31].

As shown in Fig. 5, one may see that the operating voltage increases with increasing temperature. A1 showed the lowest operating voltage (69.8 V), followed by CB1 (74.3 V), CB2 (84.8 V), A3 (85.7 V), CB3 (93.2 V), A2

Fig. 2 Textures of samples observed under a polarizing optical microscope with two crossed linear polarizers at room temperature **a** A1 (the cell gap = 7.35 μm), **b** CB1 (the cell gap = 7.28 μm)



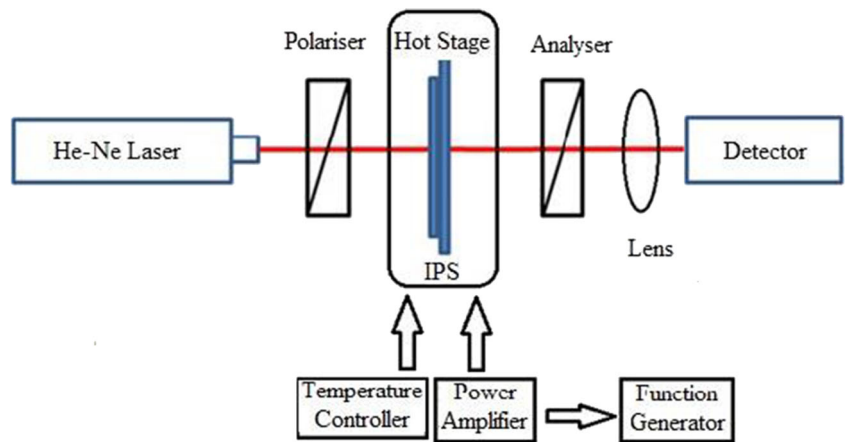
(106.6 V), and A4 (108.0 V) at 23 °C. According to these results, the operating voltage is sensitive to the monomer mass fraction of the respective cross-linker and the anchoring strength. The relative concentration of AHFF and other polymer in the precursors was adjusted to alter the strength of the polymer network. It is well known that the anchoring energy of polymer network increases as the stiffness of the polymer system increases [28]. As a result, a higher electric field is required to drive the LC molecules. Compared with the other samples, the sample A4 is harder to be driven, because the anchoring energy of polymer network formed by TMPTA and RM257 is much stronger than that of the other polymers formed by mono-monomers due to high monomer functionality even though total monomer weight is the same. TMPTA possesses three photo-crosslinking double bonds along different directions, thereby yielding their polymer networks more likely to be strong. This leads to an increase in

elastic torque of the BPLCs. Strong crosslinked polymer network in the disclination regions could limit the reorientation of LC molecules due to stronger dipole-dipole interaction with monomer molecules. The strength of polymer network decreases as the proportion of mono-functional monomers increases. Most of the monomer molecules can be polymerized inside the disclination lines. The sample A1 exhibits the lowest operating voltage, because the anchoring energy of polymer network formed by semi-rigid or flexible polymer networks monomer is the lowest one among the samples. Since fluorine atoms are smaller, leading to lower the surface tension and surface energy. In other words, the fluoroacrylate polymer offers less interaction or barrier to inside BPLC. The polar end group improves the response to an applied electric field due to its high dipole moment. The operation voltage relies on the monomer mass fraction. It decreases with increasing amount of AHFF, while it

Table 2 Phase transition temperatures of BPLC mixtures (before and after photo-stabilization) are determined by polarizing optical microscope studies

Before photo-stabilization				
Precursors	Cholesteric-blue phase (°C)	Blue phase-isotropic (°C)	Isotropic-blue phase (°C)	Blue phase-cholesteric phase (°C)
A1	78.2	84.6	82.9	80.8
A2	68.8	70.9	70.2	65.3
A3	75.9	77.3	76.9	73.5
A4	68.1	70.9	70.1	66.5
CB1	74.8	76.8	76.2	72.1
CB2	74.1	76.6	75.6	71.8
CB3	70.5	74.3	72.7	68.8
After photo-stabilization				
Samples	Cholesteric-blue phase (°C)	Blue phase-isotropic (°C)	Isotropic-blue phase (°C)	Blue phase-cholesteric phase (°C)
A1	Lower than 23	86.5	84.8	Lower than 23
A2	Lower than 23	80.1	78.4	Lower than 23
A3	Lower than 23	83.9	81.3	Lower than 23
A4	Lower than 23	79.5	77.9	Lower than 23
CB1	Lower than 23	80.1	78.5	Lower than 23
CB2	Lower than 23	79.3	77.8	Lower than 23
CB3	Lower than 23	78.7	76.3	Lower than 23

Fig. 3 Experimental setup for electro-optic measurement



increases with increasing amount of TMPTA and C12A. This difference may be owing to the polarity of end group of AHFF in the polymer network. The operating voltage of the C12A is lower than that of TMPTA for the same blend ratio with AHFF. A smaller core could be more effective than increased flexibility. The other mixing conditions were attempted a delicate balance between AHFF and other polymer to optimize the operating voltage. Therefore, the ratio of 2:2 between AHFF and C12A, TMPTA, gives a more stable structure and moderate voltage by fixing the concentration of RM257. Therefore, we infer that the trifluorophenyl of AHFF has a better molecular compatibility with polymer network, and the operating voltage reduced.

5.2 Kerr Constant

The improving target for the PSBP materials is to enhance Kerr constant to reduce the driving voltage.

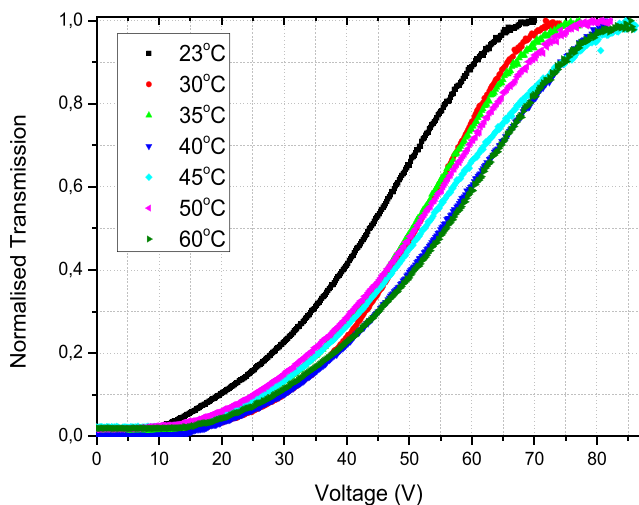
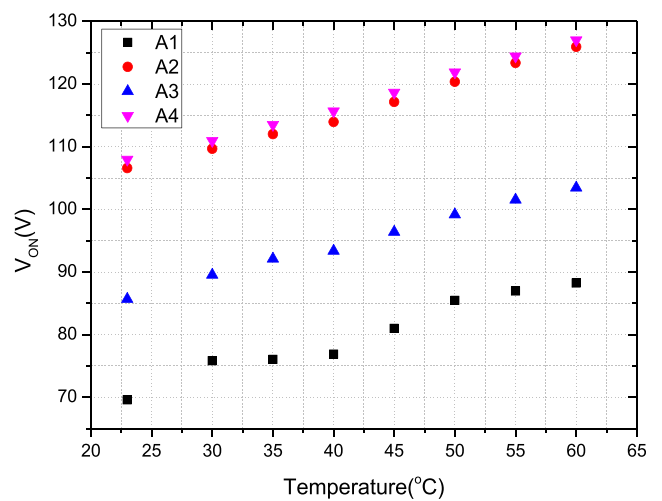
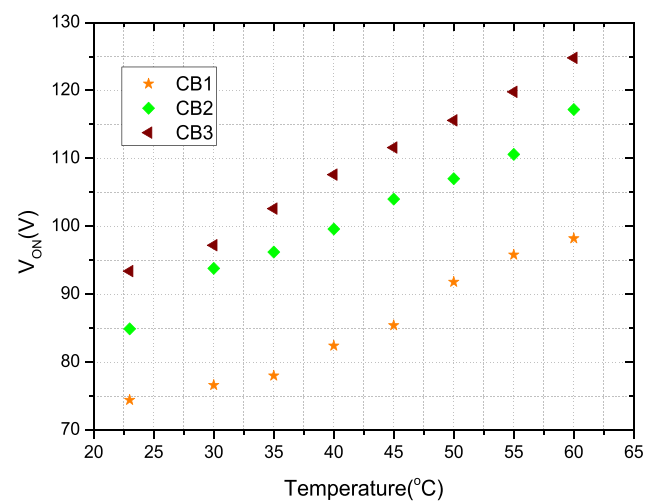


Fig. 4 Measured V-T curves in an IPS cell at different temperatures using the experimental set-up for A1, IPS cell: cell gap = 7.30 μm , electrode gap = 12 μm , and electrode width = 8 μm

Macroscopically, BPLC is an isotropic Kerr medium when there is no external electric field present. As electric field increases, the BPLC becomes anisotropic along



(a)



(b)

Fig. 5 The operating voltage as a function of temperature for different concentrations of AHFF compound

the electric field direction. The refractive index change follows the Kerr effect in the low field region but gradually saturates as the electric field keeps increasing, which can be well explained by an extended Kerr effect [55]. The $\Delta n_{\text{induced}}$ in the weak field region is related to E , wavelength λ , and Kerr constant K as

$$\Delta n_{\text{induced}} = \lambda K E^2 \quad (2)$$

According to the extended Kerr effect, the $\Delta n_{\text{induced}}$ of PSBPLCs is related to the electric field [55].

$$\Delta n_{\text{induced}}(E) = \Delta n_s \left(1 - \exp \left[- \left(\frac{E}{E_s} \right)^2 \right] \right) \quad (3)$$

where Δn_s is the saturated induced birefringence and E_s is the saturation electric field. In the weak field region ($E \ll E_s$), the Kerr constant is derived as follows [56]

$$K \frac{\Delta n_s}{\lambda E_s^2} \approx \Delta n \Delta \varepsilon \frac{p^2}{\lambda k (2\pi)^2} \quad (4)$$

where $\Delta \varepsilon$, p , and k are the dielectric anisotropy, the pitch length, and the effective elastic constant of this system, respectively. Based on Equation (3), the Kerr constant was obtained by fitting the VT curves with the extended Kerr effect model, since the $\Delta n_{\text{induced}}$ should be saturated in the strong electric field. Figure 6 exhibits the Kerr constant consisting of different AHFF concentration in the systems. A1 showed the largest Kerr constant (9.4 nm/V²), followed by CB1 (7.8 nm/V²), A3 (5.8 nm/V²), CB2 (5.3 nm/V²), CB3 (4.8 nm/V²), A2 (3.9 nm/V²), and A4 (3.7 nm/V²) at 23 °C. A decrease in required applied voltage corresponds to an increased Kerr constant. Among the samples, the Kerr constant of sample A4 is the smallest one, since the strong anchoring polymer network that cannot respond to readily the re-orientation of LC molecules in an external field decreases the Kerr constant due to the increase of polymer interface. Another alternative reason for the decreased Kerr constants is the increase of the effective elastic constant governed by both the polymer anchoring force. The increased effective elastic constant is believed to originate from the TMPTA. Besides, the Kerr constants decrease with increasing temperature. The low molecular weight crosslink monomers are able to reduce the strength of polymer network and lower the interfacial energy at the interface between the polymer network and the double twist cylinders enhancing the Kerr constant. The enhancement of the Kerr coefficient may be owing to the weak anchoring nature of AHFF originating from the flexibility and polar group. Nitro-benzene in a liquid state is generally known to show large Kerr constants, $K = 24 \times 10^{-12} \text{ V}^{-2} \text{ m}$. However, the values of the

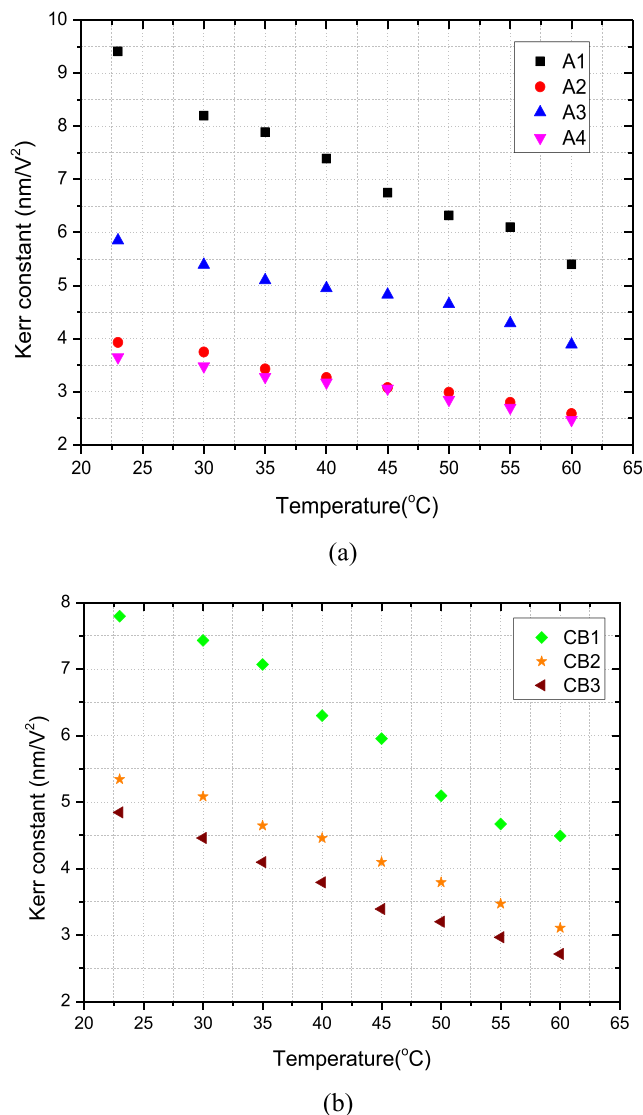


Fig. 6 Temperature dependence of Kerr coefficient of PSBPs for different concentrations of AHFF compound

Kerr constant in the precursors are the order of $10^{-10} - 10^{-9} \text{ V}^{-2} \text{ m}$, which is about 100–1000 times larger than those of conventional Kerr materials for instance nitrobenzene [62]. This value is comparable with that in a PSBPLC [32–39]. If the wavelength was decreased, Kerr constant would increase so that the required operating voltage would be lower at a shorter wavelength, since a larger wavelength displays a shorter phase retardation under the same driving voltage and the induced birefringence decreases as the wavelength increases under normal dispersion conditions [50].

5.3 Response Time

Microsecond gray-to-gray response time is one of the major properties of BPLC in comparison with conventional nematic

LCs. Decay and rise times can be expressed, respectively, as [41]

$$T_{\text{decay}} = \frac{\gamma_1}{E_c^2 \epsilon_o \Delta \epsilon} \tag{5}$$

$$T_{\text{rise}} = \frac{T_{\text{decay}}}{(V/V_c)^2 - 1} \tag{6}$$

Here, V_c is the critical voltage in order to unwind the BPLC pitches, γ_1 is the rotational viscosity, and E_c is the critical electric field.

Figure 7 displays the temperature dependence of the decay processes for the PSBPs consisting of various ratios of polymer. The rise time is not included here because of being highly dependent on the applied voltage. The decay time was determined from 90 to 10% transmittance change. Response time is highly related to the stability of the samples. The fast response time originates from the short pitch length, LC host, and strong crosslinking polymer network [25, 26]. All the measurements were conducted at different temperatures. As seen in Fig. 7, the decay processes decrease with increasing temperature. As a result, the decay time is reduced from millisecond to sub millisecond. A4 showed the lowest decay time (0.468 ms), followed by A2 (0.598 ms), A3 (0.975 ms), CB3 (1.440 ms), A1 (1.782 ms), CB2 (3.261 ms), and CB1 (3.822 ms) at 23 °C. These times are comparable with those published in the literature [34–41]. The higher monomer concentration of TMPTA gives a faster response time. Therefore, a more stable sample tends to have a faster response time. As the concentration of C12A increases and that of AHFF decreases in the precursors, the decay time of PSBPLC decreases. Electro-optic response is very fast in the region of local director reorientation and is not almost affected by the magnitude of electric fields although the response becomes very slower as the electric field increased in the region of electrostriction, since the local BPLC directors within DTCs are unwound more seriously under a stronger electric field. Thus, upon removal of electric field, it takes longer time for those BPLC directors to relax back to their original DTCs, leading to longer response time. Therefore, these results could be well explained by a report that the local director reorientation preferentially occurred in PSBPs. In addition, HTG-135200 possesses a relatively high viscosity owing to its $\Delta \epsilon$.

5.4 Hysteresis

Hysteresis is a main issue that influences the gray scale in LC displays and it must be less than 5% prior to the wide application of PSBPLCs [27]. To measure the hysteresis of our IPS devices, the IPS devices were driven by increasing the applied voltage upwards to the operating voltage and then gradually

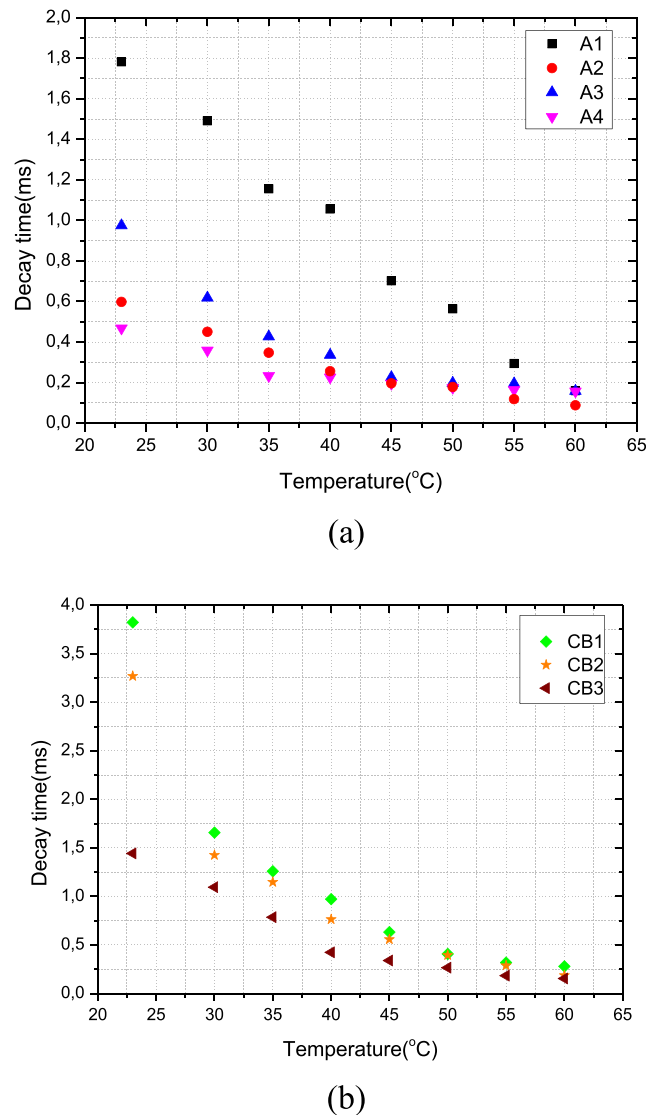


Fig. 7 Temperature dependence of electro-optical decay time for different concentrations of AHFF compound

decreasing downwards to zero. The hysteresis is defined by the voltage difference between the upward and downward scans at half of the peak transmittance. The electric fields near electrode edges in an IPS mode are particularly strong. They may cause lattice deformation, thereby generating hysteresis. Higher operating voltage gives rise to a more distinguishable hysteresis, which is ascribed to the lattice distortions of the PSBPLC. Hysteresis mechanism is controlled by the relaxation ability of BPLC, steric hindrance of polymer network, and their anchoring force with each other. Therefore, both the BPLC lattice and the polymer network cannot completely relax to their original states and created large hysteresis.

Figure 8 demonstrates the hysteresis of PSBPLCs obtained under different concentrations of AHFF compound. The hysteresis showed the highest in CB2 (6.07%) and it decreased as the following order CB1 (5.90%), A1 (5.88%), CB3 (5.13%),

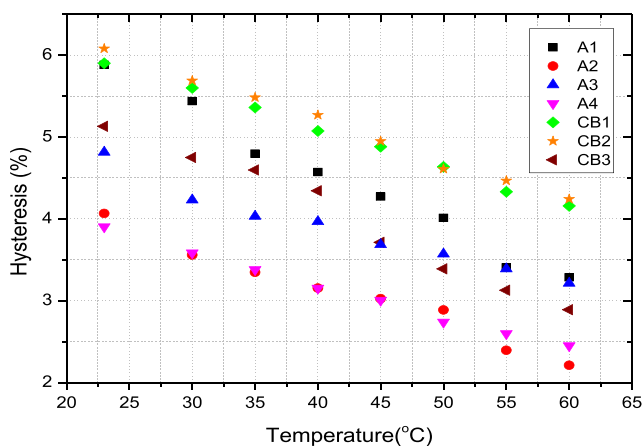


Fig. 8 Temperature dependence of voltage hysteresis for different concentrations of AHFF compound

A3 (4.81%), A2 (4.06%), and A4 (3.9%) at 23 °C. Additionally, the hysteresis decreases with increasing temperature. In other words, hysteresis is relatively sensitive to temperature and the monomer concentration. The reduction in hysteresis may give rise to the reduction in viscosity with an increase in temperature [25]. Among the samples, the hysteresis of sample A4 is the lowest one due to the largest surface anchoring energy of the polymer system formed by TMPTA. As the applied voltage decreases, the LC molecules can recover to their original state by the large anchoring energy of polymer network. As the concentration of C12A increases and AHFF decreases in the precursor, the hysteresis of PSBPLC increases. The larger hysteresis results from the lower anchoring energy of the more flexible polymer network, since the low interfacial energy makes it difficult to recover the original alignment of LC when the applied voltage is reduced. All experiment results were summarized in Table 3.

Table 3 Electro-optic properties of PSBPLC composites at 23 °C, $\lambda = 633$ nm

Sample	Operating voltage (V)	Kerr constant (nm/V ²)	Decay time (ms)	Hysteresis (%)
A1	69.8	9.4	1.782	5.88
A2	106.6	3.9	0.598	4.86
A3	85.7	5.8	0.950	4.81
A4	108.0	3.7	0.468	3.90
CB1	74.3	7.8	3.820	5.90
CB2	84.2	5.3	3.261	6.07
CB3	93.2	4.8	1.440	5.13

6 Conclusion

The polymer structure within the PSBPLC influences the thermal stability and electro-optical properties. Optimization of materials plays an important role for advancing the technology. Therefore, we have reported a newly synthesized ultraviolet-polymerizable reactive monomer containing trifluorophenyl. We successfully broadened the temperature range of the PSBPLC as well as achieved lower driving voltage, faster response time, lower hysteresis, and higher Kerr constant by optimizing the combination of various functional monomer and new monomer. The operation voltage decreases with increasing the concentration of the new monomer. The experimental results indicate that the electro-optical properties of PSBPLC can be improved simultaneously by polymer system with polar end group, which are the most promising candidates for decreasing the operating voltage of the BP system.

Acknowledgments This research was supported by grants from the Scientific and Technological Research Council of Turkey (TUBITAK) to N. Avci.

Funding This research was supported by grants from the Scientific and Technological Research Council of Turkey (TUBITAK) to N. Avci.

Compliance with Ethical Standards

Conflict of Interest The authors declare that they have no conflict of interest.

References

1. F. Reinitzer, Beiträge zur Kenntniss des Cholesterins. Monatshefte für Chemie (Wein), 9, 421–441 (1888). Translation: contributions to the understanding of cholesterol. *Liq. Cryst.* **5**, 7–18 (1989)
2. P.P. Crooker, in *Chirality of liquid crystals*, ed. by H.-S. Kitzerow, C. Bahr. Blue phases (Springer-Verlag, New York, 2001), pp. 186–222
3. H. Kikuchi, Liquid crystalline blue phases. *Struct. Bond.* **128**, 99–117 (2008)
4. H. Kikuchi, M. Yokota, Y. Hisakado, et al., Polymer stabilized liquid crystal blue phases. *Nat. Mater.* **1**, 64–68 (2002)
5. H.J. Coles, M.N. Pivnenko, Liquid crystal blue phases with a wide temperature range. *Nat. Mater.* **436**, 997–1000 (2005)
6. I. Dierking, W. Blenkhorn, E. Credland, W. Drake, R. Kociuruba, B. Kayser, T. Michael, Stabilising liquid crystalline blue phases. *Soft Matter.* **8**, 4355–4362 (2012)
7. H. Yoshida, Y. Tanaka, K. Kawamoto, et al., Nanoparticle-stabilized cholesteric blue phases. *Appl. Phys. Express* **2**, 121501 (2009)
8. L. Wang, W. He, X. Xiao, et al., Hysteresis free blue phase liquid crystal stabilized by ZnS nanoparticles. *Small* **8**, 2189–2193 (2012)
9. M. Lavrič, G. Cordoyiannis, S. Kralj, et al., Effect of anisotropic MoS₂ nanoparticles on the blue phase range of a chiral liquid crystal. *Appl. Opt.* **52**, 47–52 (2013)

10. E. Karatairi, B. Rožič, Z. Kutnjak, et al., Nanoparticle-induced widening of the temperature range of liquid-crystalline blue phases. *Phys. Rev. E* **81**, 041703–1–5 (2010)
11. W. He, G. Pan, Z. Yang, D. Zhao, G. Niu, W. Huang, X. Yuan, J. Guo, H. Cao, H. Yang, Wide blue phase range in a hydrogen-bonded self-assembled complex of chiral fluoro-substituted benzoic acid and pyridine derivative. *Adv. Mater.* **21**, 2050–2053 (2009)
12. I. Gvozдовskyy, Blue phases' of highly chiral thermotropic liquid crystals with a wide range of near-room temperature. *Liq. Cryst.* **42**, 1391–1404 (2015)
13. A. Yoshizawa, M. Sato, J. Rokunohe, A blue phase observed for a novel chiral compound possessing molecular biaxiality. *J. Mater. Chem.* **15**, 3285–3290 (2005)
14. S. Taushanoff, K.V. Le, J. Williams, et al., Stable amorphous blue phase of bent-core nematic liquid crystals doped with a chiral material. *J. Mater. Chem.* **20**, 5893–5898 (2010)
15. M. Lee, S.-T. Hur, H. Higuchi, et al., Liquid crystalline blue phase I observed for a bent-core molecule and its electro-optical performance. *J. Mater. Chem.* **20**, 5813–5816 (2010)
16. H. Wang, Z. Zheng, D. Shen, Blue phase liquid crystals induced by bent-shaped molecules based on 1,3,4-oxadiazole derivatives. *Liq. Cryst.* **39**, 99–103 (2012)
17. K.-W. Park, M.-J. Gim, S. Kim, et al., Liquid-crystalline blue phase II system comprising a bent-core molecule with a wide stable temperature range. *Appl. Mater. Interfaces* **5**, 8025–8029 (2013)
18. Z. Zheng, D. Shen, P. Huang, Wide blue phase range of chiral nematic liquid crystal doped with bent-shaped molecules. *New J. Phys.* **10**, 113018–1–10 (2010)
19. A. Yoshizawa, Y. Kogawa, K. Kobayashi, Y. Takanishi, J. Yamamoto, A binaphthyl derivative with a wide temperature range of a blue phase. *J. Mater. Chem.* **19**, 5759–5764 (2009)
20. X. Chen, L. Wang, C. Li, J. Xiao, H. Ding, X. Liu, X. Zhang, W. He, H. Yang, H. Yang, Light-controllable reflection wavelength of blue phase liquid crystals doped with azobenzene-dimers. *Chem. Commun.* **49**(86), 10097–10099 (2013)
21. A. Hauser, M. Thieme, A. Saupe, G. Heppke, D. Krüerke, Surface-imaging of frozen blue phases in a discotic liquid crystal with atomic force microscopy. *J. Mater. Chem.* **7**(11), 2223–2229 (1997)
22. P. Lin, Q. Yan, Z. Wei, et al., All-inorganic perovskite quantum dots stabilized blue phase liquid crystals. *Optics express* **26**(14), 18310–18319 (2018)
23. W. Zhang, X. Wang, D. Wang, Z. Yang, H. Gao, Y. Xing, W. He, H. Cao, H. Yang, Blue phase liquid crystals affected by graphene oxide modified with aminoazobenzol group. *Liq. Cryst.* **43**(5), 573–580 (2016)
24. Y. Zhao, X.X. Qiao, K. Li, et al., Blue phase liquid crystals stabilized by graphene oxide modified with aminoalkyl group. *Molecular Crystals and Liquid Crystals* **664**(1), 1–8 (2018)
25. J. Yan, S.-T. Wu, Polymer-stabilized blue phase liquid crystals: A tutorial [invited]. *Opt. Mater. Express* **1**, 1527–1535 (2011)
26. Y.Y. Chen, S.-T. Wu, Recent advances on polymer-stabilized blue phase liquid crystal materials and devices. *J. Appl. Polym. Sci.* **131**, 40556 (2014)
27. L. Rao, Z. Ge, S.-T. Wu, et al., Low voltage blue-phase liquid crystal displays. *Appl. Phys. Lett.* **95**, 231101 (2009)
28. J. Yan, L. Rao, M. Jiao, Y. Li, H.C. Cheng, S.T. Wu, Polymer-stabilized optically isotropic liquid crystals for next generation display and photonics applications. *J. Mater. Chem.* **21**, 7870–7877 (2011)
29. Z. Ge, S. Gauza, M. Jiao, et al., Electro-optics of polymer-stabilized blue phase liquid crystal displays. *Appl. Phys. Lett.* **94**(10), 101104 (2009)
30. Z. Ge, L. Rao, S. Gauza, et al., Modeling of blue phase liquid crystal displays. *J. Disp. Technol.* **5**, 250–256 (2009)
31. L. Rao, Z. Ge, S. Gauza, et al., Emerging liquid crystal displays based on the Kerr effect. *Mol. Cryst. Liq. Cryst.* **527**, 30–42 (2010)
32. K.-M. Chen, S. Gauza, H. Xianyu, et al., Hysteresis effects in blue phase liquid crystals. *J. Disp. Technol.* **6**, 318–322 (2010)
33. J.L. Zhu, S.B. Ni, Y. Su, et al., The influence of polymer system on polymer-stabilised blue phase liquid crystals. *Liq. Cryst.* **41**, 891–896 (2014)
34. J.L. Zhu, S.B. Ni, Y. Song, et al., Improved Kerr constant and response time of polymer-stabilized blue phase liquid crystal with a reactive diluent. *Appl. Phys. Lett.* **102**, 071104 (2013)
35. T.-N. Oo, T. Mizunuma, Y. Nagano, et al., Effects of monomer/liquid crystal compositions on electro-optical properties of polymer-stabilized blue phase liquid crystal. *Opt. Mat. Express* **1**, 1502–1510 (2011)
36. J. Yan, Y. Chen, S.-T. Wu, et al., Dynamic response of a polymer-stabilized blue-phase liquid crystal. *J. Appl. Phys.* **111**, 063103 (2012)
37. H. Kikuchi, Y. Hisakado, K. Uchida, et al., Fast electro-optical effect in polymer-stabilized blue phases. *Proc. SPIE* **5518**, 182–189 (2004)
38. H. Yoshida, H. Kikuchi, T. Nagamura, et al., Large electro-optic Kerr effect in polymer-stabilized liquid-crystalline blue phases. *Adv. Mater.* **17**, 96–98 (2005)
39. J. Xiang, O.D. Lavrentovich, Blue-phase-polymer-templated nematic with sub-millisecond broad-temperature range electro-optic switching. *Appl. Phys. Lett.* **103**, 051112–1–4 (2013)
40. H. Choi, H. Higuchi, H. Kikuchi, Electro-optic response of liquid crystalline blue phases with different chiral pitches. *Soft Matter* **7**, 4252–4256 (2011)
41. K.M. Chen, S. Gauza, S.-T. Wu, et al., Submillisecond gray-level response time of a polymer-stabilized blue-phase liquid crystal. *J. Disp. Technol.* **6**, 49–51 (2010)
42. P.J. Hsieh, H.M. Chen, Hysteresis-free polymer-stabilised blue phase liquid crystals comprising low surface tension monomers. *Liq. Cryst.* **42**(2), 216–221 (2015)
43. L. Gao, X. Li, X.W. Du, W.M. Han, C.Y. Chen, J.L. Zhu, Y.J. Zhang, Y.B. Sun, High dielectric polymer and its application on electro-optical Kerr effect of blue phase liquid crystal. *Appl. Phys. Lett.* **113**(22), 221907 (2018)
44. L. Rao, J. Yan, S.-T. Wu, et al., A large Kerr constant polymer-stabilized blue phase liquid crystal. *Appl. Phys. Lett.* **98**, 081109 (2011)
45. Y. Chen, D. Xu, S.-T. Wu, S.T. Wu, S.I. Yamamoto, Y. Haseba, A low voltage and submillisecond-response polymer-stabilized blue phase liquid crystal. *Appl. Phys. Lett.* **102**, 141116 (2013)
46. D. Xu, J. Yan, J. Yuan, F. Peng, Y. Chen, S.T. Wu, Electro-optic response of polymer-stabilized blue phase liquid crystals. *Appl. Phys. Lett.* **105**, 011119 (2014)
47. J. Yan, S.-T. Wu, Effect of polymer concentration and composition on blue phase liquid crystals. *J. Display Tech.* **7**, 490–493 (2011)
48. J. Li, W. Du, A. Gao, et al., Enlarging the Kerr constant of polymer-stabilised blue phases with a novel chiral monomer. *Liq. Cryst.* **43**(7), 937–943 (2016)
49. Y. Li, Y. Chen, J. Sun, et al., Dielectric Dispersion on the Kerr Constant of Blue Phase Liquid Crystals. *Appl. Phys. Lett.* **99**(18), 181126 (2011)
50. M. Jiao, Y. Jin, S.-T. Wu, Dispersion Relation on the Kerr Constant of a Polymer-Stabilized Optically Isotropic Liquid Crystal. *Phys. Rev. E* **83**(4), 041706 (2011)

51. F. Peng, Y. Chen, J. Yuan, H. Chen, S.T. Wu, Y. Haseba, Low temperature and high frequency effects on polymer-stabilized blue phase liquid crystals with large dielectric anisotropy. *J. Mater. Chem. C* **2**, 3597–3601 (2014)
52. K. Kishikawa, T. Watanabe, M. Kohri, T. Taniguchi, M. Takahashi, S. Kohmoto, Effect of the number of chiral mesogenic units and their spatial arrangement in dopant molecules on the stabilisation of blue phases. *Liq. Cryst.* **41**(6), 839–849 (2014)
53. A.C. Pawsey, P.S. Clegg, Colloidal particles in blue phase liquid crystals. *Soft Mater.* **11**, 3304–3312 (2015)
54. H.Y. Chen, H.H. Liu, J.L. Lai, C.H. Chiu, J.Y. Chou, Relation between physical parameters and thermal stability of liquid-crystal blue phase. *Appl. Phys. Lett.* **97**, 181919 (2010)
55. J. Yan, H.C. Cheng, S. Gauza, Y. Li, M. Jiao, L. Rao, S.T. Wu, Extended Kerr effect of polymer-stabilized blue-phase liquid crystals. *Appl. Phys. Lett.* **96**, 071105 (2010)
56. P.R. Gerber, Electro-optical effects of a small-pitch blue-phase system. *Mol. Cryst. Liq. Cryst.* **116**, 197–206 (1985)
57. R. Manda, M.S. Kim, E.J. Shin, et al., Phase stabilisation of blue-phase liquid crystals using a polymerisable chiral additive. *Liq. Cryst.* **44**(6), 1059–1068 (2017)
58. N. Avci, The influence of diluter system on polymer-stabilised blue-phase liquid crystals. *Liq. Cryst.* **45**(3), 459–467 (2018)
59. L.L. Tian, F. Chu, H. Dou, X. Zhou, Q.H. Wang, A transfective polymer-stabilised blue-phase liquid display with partitioned wall-shaped electrodes. *Liq. Cryst.* **45**(8), 1259–1263 (2018)
60. D.P. Zhu, B.H. Chen, Z. Chen, et al., Low-voltage polymer-stabilised blue-phase liquid crystals with oleic acid (OA)-modified LaF₃ nanoparticles. *Liq. Cryst.* **45**(11), 1654–1660 (2018)
61. B.H. Chen, D.P. Zhu, F.Y. Huo, et al., Influence of Monomer Structure on the Properties of Blue Phase Liquid Crystal. *Liquid Cryst.* **45**(11), 1637–1643 (2018)
62. E. Hecht, *Optics* (Addison Wesley, Reading, MA, 2002), pp. 318–320

Publisher's Note Springer Nature remains neutral with regard to jurisdictional claims in published maps and institutional affiliations.